Received: 12 December 2020 | Revised: 8 March 2021 | Accepted: 10 March 2021

DOI: 10.1002/er.6695

RESEARCH ARTICLE

INTERNATIONAL JOURNAL OF ENERGY RESEARCH WILEY

# First-principles calculations of structural, electronic, optical, and thermoelectric properties of ternary *d*-metal sulfides $Sc_2CdS_4$ and $Y_2CdS_4$ compounds

**Abdul Ahad Khan**[1] | **Ali H. Reshak**[2,3,4] | **Zubaida Noor**[5] | **Ghulam Murtaza**[5,6] | **Murefah Mana Al-Anazy**[7] | **Hind Althib**[8,9] | **Tahani H. Flemban**[8,9] | **Amel Laref**[10] | **AM Mustafa Al Bakri**[4] | **Jiri Bila**[3]

[1]Department of Physics, University of the Peshawar, Peshawar, Pakistan

[2]Physics Department, College of Science, University of Basrah, Basrah, Iraq

[3]Department of Instrumentation and Control Engineering, Faculty of Mechanical Engineering, CTU in Prague, Prague, Czech Republic

[4]Center of Excellence Geopolymer and Green Technology (CEGeoGTech), University Malaysia Perlis, Kangar, Malaysia

[5]Materials Modeling Lab, Department of Physics, Islamia College Peshawar, Peshawar, Pakistan

[6]Department of Mathematics & Natural Sciences, Prince Mohammad Bin Fahd University, Alkhobar, Kingdom of Saudi Arabia

[7]Department of Chemistry, College of Science, Princess Nourah bint Abdulrahman University, Riyadh, Saudi Arabia

[8]Basic and Applied Scientific Research Center, Imam Abdulrahman Bin Faisal University, Dammam, Saudi Arabia

[9]Department of Physics, College of Science, Imam Abdulrahman Bin Faisal University, Dammam, Saudi Arabia

[10]Department of Physics and Astronomy, College of Science, King Saud University, Riyadh, Kingdom of Saudi Arabia

**Correspondence**
Ali H. Reshak, Department of Instrumentation and Control Engineering, Faculty of Mechanical Engineering, CTU in Prague, Technicka 4, Prague 6 166 07, Czech Republic.
Email: maalidph@yahoo.co.uk

**Funding information**
Deanship of Scientific Research, King Saud University

## Summary

Direct energy bandgap materials are crucial for efficient optoelectronics devices. Therefore, investigating new direct gap materials is important. In the present work, two novel *d*-metal sulfides $Sc_2CdS_4$ and $Y_2CdS_4$ compounds are investigated by using the all-electron full-potential linearized augmented plane-wave method. The energy optimization predicts lattice constants 10.85 and 11.31 Å for $Sc_2CdS_4$ and $Y_2CdS_4$, respectively. Both the compounds show semiconducting nature and direct bandgap with a value of 1.886 eV for $Sc_2CdS_4$ and 2.209 eV for $Y_2CdS_4$. Strong hybridization between S-*p* and Sc/Y-*d* orbitals is present among valence and conduction bands, which is beneficial to electrical transport. Key optical parameters are calculated. The static value of the reflectivity $R(0)$ and refractive index $n(0)$ varies inversely with the energy bandgap ($E_g$). Both the compounds $Sc_2CdS_4$ and $Y_2CdS_4$ are P-type thermoelectric materials because the holes carriers dominate the electronic transport. Both the compounds reveal figure of merit of about 0.5. Appropriate direct energy gap and figure of merit indicate the possible applications of these compounds for energy conversion devices.

**KEYWORDS**

*d*-metal sulfides, optical analysis, P-type thermoelectrics

  

## 1 | INTRODUCTION

The world is quickly turning into a global village because of the expanding everyday prerequisite of energy. The requirement for energy and its related services to fulfill human social and economic development, government assistance, and health is increasing. Getting back to renewable energy to help alleviate environmental degradation is a wonderful methodology, which should be feasible in order to satisfy the energy demands of the future generation. Sustainable power resources are fundamental for the continued life because of the quick utilization of fossil fuels on earth. One of the perfect clean energy strategies is to utilize the solar cells for the purpose of converting light energy into electricity.[1]

Semiconductors with a bandgap in the energy range of ~1.5 eV are perfectly considered as ideal materials for the development of solar cell with high proficiency.[1] Moreover, the successful optoelectronic devices could be investigated with appropriate bandgap choice by focusing on the energy range. The appropriate energy bandgap is the direct one where the immediate transition from valence to conduction band is possible for productive optoelectronic applications. It is, therefore, necessary to find new materials with the ideal properties to fulfill the needs of the rapidly developing innovation.[2]

The spinel materials $X_2YZ_4$, with both $X$ and $Y$ are metallic elements and $Z$ belongs to (O, S, Se, Te) chalcogenides family, have motivated various investigations,[3,4] since it exhibited significant physical properties, that is, phase transformations,[5] half metallicity,[6] colossal magnetoresistance,[7] metal-to-insulator transitions,[8] thermoelectricity,[9] thermodynamic stability,[10] charge storage ordering,[11] transparent character for longer energy range,[12] nonlinear optical susceptibility,[13] and so on, which make them promising candidates for assembling optoelectronic devices and materials for various applications, especially in magnetism, geophysics, catalysis, and environmental protection.[14-18] The thiospinels could be utilized for various applications in the field of defect engineering by implementing pressure in specific manners.[19]

Peskov et al reported the crystal chemical characterization of $d$-metal sulfides/selenides/tellurides containing discrete tetrahedral $TX_4$(X = S, Se, Te) groups with chalcogen anions.[19,20] The randomly scattered atoms in chalcogenides involve diverse crystallographic positions that were not included initially in the sample. Thus, they obtained an information base containing structural information on 122 $d$-metal compounds with the formula $M_y[TX_4]$ (where M represents metal and $y = 2$ to 6). In these compounds, the mechanisms behind the interatomic bonds were majorly resolved with the help of AutoCN program.[20]

Different types of materials have been predicted for energy harvesting applications; Muhammad et al investigated different concentrations of hydrogen in the mesh of nitrogen-doped graphene networks using the pseudopotential scheme.[21] In another work,[22] the authors have doped different group II metals. They have also calculated the magnetic moments and also reported the optical properties of the doped systems using the random phase approximation. Furthermore, 3D transition metals tetraoxide superhalogen clusters incorporated single and divacancy monolayer graphene was studied by density functional theory (DFT).[23] Thin film solar cells (TFSCs) have been vastly investigated in recent times.[24] TFSCs show high efficiency in solar cell applications. However, comparatively less attention has been paid to the optoelectronic applications of spinel compounds.[25]

Despite important research on thiospinels, other compounds like $Sc_2CdS_4$ and $Y_2CdS_4$ usually received less attention and are not studied yet. Regarding these compounds, there is a lack of theoretical data on the understudy materials. First-principles calculations assist in understanding the materials' properties without the availability of any experimental data. This investigation was expected to locate the fundamental physical and structural properties of $Sc_2CdS_4$ and $Y_2CdS_4$ compounds. In this work, first-principles calculations of structural, electronic, optical, and thermoelectric properties of ternary $d$-metal sulfides $Sc_2CdS_4$ and $Y_2CdS_4$ compounds are investigated under the framework of DFT. Furthermore, the work is significant due to its novelty and it delivers new results that have appropriate features for their use in advanced applications.

## 2 | COMPUTATIONAL DETAILS

Different physical properties of the $d$-metal sulfides $Sc_2CdS_4$ and $Y_2CdS_4$ have been calculated using the state-of-the-art density functional calculations. The full potential scheme of linearized augmented plane-wave plus local orbitals is used as implemented in the Wien2K computer package.[26] The maximum angular momentum value of $l = 12$ for the charge and potential expansion in spherical harmonics is used. The radii of the muffin tin spheres are 2.21, 2.25, 2.50, and 2.15 Bohr for Sc, Y, Cd, and S, respectively. For the interstitial region, the plane-wave cutoff value ($Kmax = 8.0/RMT$) was used and 1000 k-points is used for the Brillouin zone integrations. For the determination of structural parameters of the materials, the generalized gradient

approximation (GGA)[27] is used. On the other hand, the new semi-local potential known as the "Tran and Blaha modified Becke-Johnson" TB-mBJ[28] potential is used for the calculation of electric structure due to its better energy bandgap prediction compared to other less computational potentials.

## 3 | RESULTS AND DISCUSSION

### 3.1 | Structural properties

The ternary *d*-metal sulfides $Sc_2CdS_4$ and $Y_2CdS_4$ compounds exist in cubic structure with crystallographic parameters $a = b = c$, $\alpha = \beta = \gamma = 90°$, and space group $Fd\bar{3}m$ (#227). The relaxed crystal structure (left) of the title compounds and $CdS_4$ tetrahedron (right) is shown in Figure 1. In this structure, each Cd atom is tetrahedrally coordinated by four sulfur atoms, while Sc/Y atom is coordinated with six sulfur atoms. Using the experimental/estimated lattice constant through self-consistent manner, structural relaxation of internal parameters is performed. The basic structure parameters of the compounds are determined by performing volume optimization.

Table 1 depicts the calculated relaxed values of these parameters for both the compounds. The lattice constant increased in the order of Sc → Y; it is 10.85 Å for $Sc_2CdS_4$ and 11.31 Å for $Y_2CdS_4$ by changing the cation. It is noticed that the lattice constant, unit cell volume, and the bond length increase by replacing Sc with Y. This increase is due to the fact that Sc has larger atomic size than the Y element.

### 3.2 | Electronic properties

#### 3.2.1 | Energy band structure

The calculated electronic band structures of $Sc_2CdS_4$ and $Y_2CdS_4$ compounds are displayed in Figure 2, in the high symmetry direction W-L-Γ-X-W-K in the first Brillouin zone. The energy range is set from −5 to 5 eV and the Fermi level is considered as reference (0 eV). Both the compounds show semiconducting nature and direct bandgap with a value of 1.886 eV for $Sc_2CdS_4$ and 2.209 eV for $Y_2CdS_4$, respectively. The increase in the bandgap is caused by the replacement of lower atomic radius cation with the higher one. Bond length increased (shown in Table 1) by the cation replacement, which shows higher energy bandgap of these compounds. Despite no experimental value of the compounds is available in the literature, we believe that these values are more accurate and could be closer to the measured bandgap of the materials.

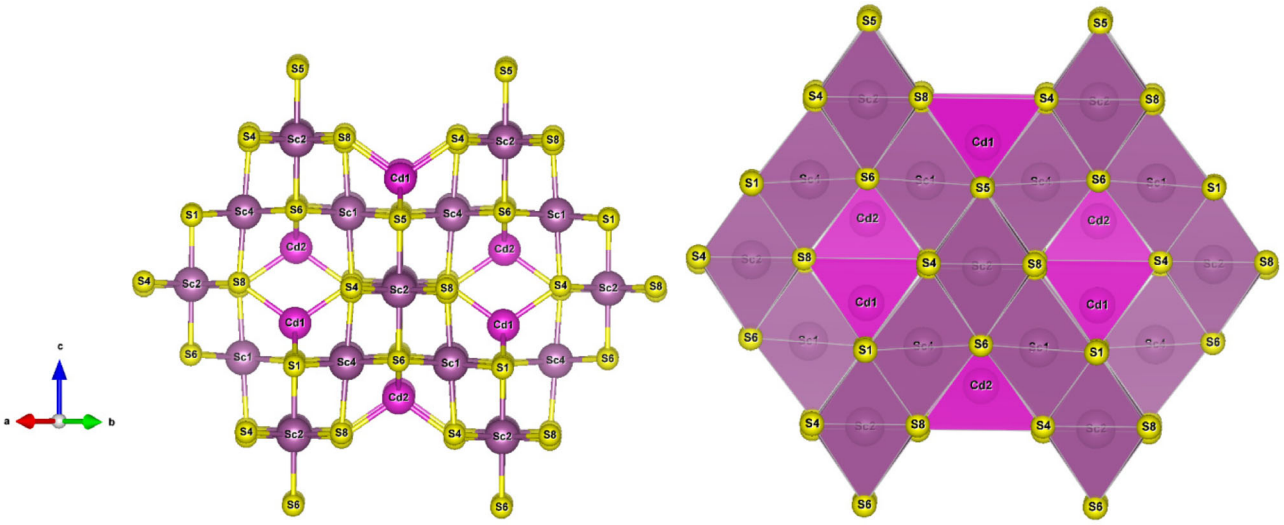


**FIGURE 1** Relaxed crystal structure (left) and polyhedron (right) of $Sc_2CdS_4$ compound [Colour figure can be viewed at wileyonlinelibrary.com]

**TABLE 1** The calculated lattice constants *a*, *b*, and *c* (in Å), bond angle *α*, *β*, and *γ*, bond lengths *d* (in Å), and optimize volume (in a.u$^3$), for $Sc_2CdS_4$ and $Y_2CdS_4$ compounds

| Compounds | $a = b = c$ | $\alpha = \beta = \gamma$ | $V_o$ | $d$ | |
|---|---|---|---|---|---|
| $Sc_2CdS_4$ | 10.85 | 90 | 1278.91 | 2.552[Cd-S] | 2.602[Sc-S] |
| $Y_2CdS_4$ | 11.31 | 90 | 1447.46 | 2.596[Cd-S] | 2.746[Y-S] |

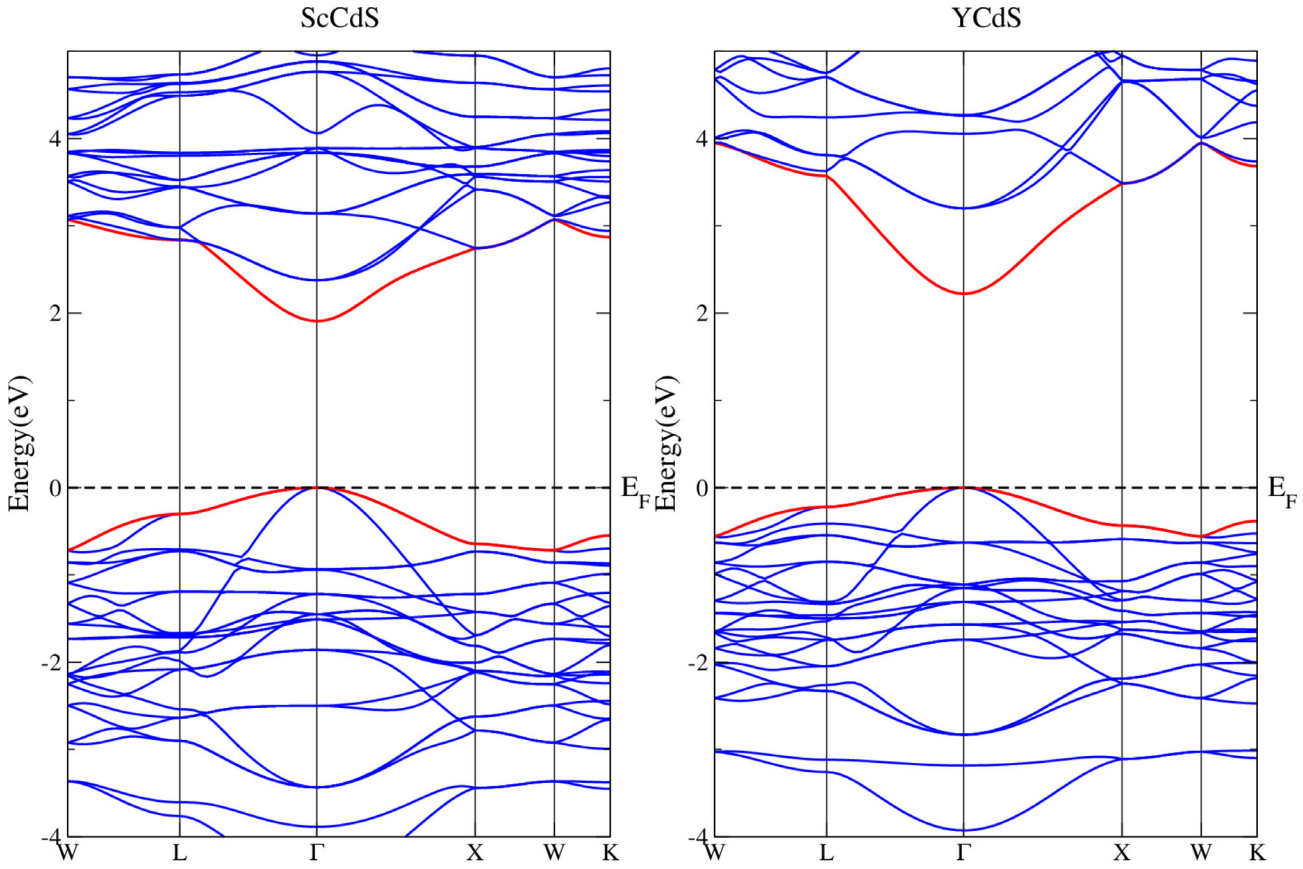


FIGURE 2 Energy band structure calculated by mBJ of $Sc_2CdS_4$ and $Y_2CdS_4$ compounds [Colour figure can be viewed at wileyonlinelibrary.com]

TABLE 2 The calculated effective masses of the compounds (in units of a.m.u)

| Compounds | Electron effect mass ($m_e^*$) | Hole effective mass ($m_h^*$) |
|---|---|---|
| $Sc_2CdS_4$ | $0.0678*10^{-31}$ | $0.2339*10^{-31}$ |
| $Y_2CdS_4$ | $0.0575*10^{-31}1$ | $0.2823*10^{-31}$ |

The effective mass of the compounds is also calculated from the bands structure at the Γ symmetry point. From Table 2, it is clear that the electron effective masses are less than the hole's effective masses. Furthermore, $Y_2CdS_4$ has higher holes effective mass and lower electron effective mass compared to $Sc_2CdS_4$ due to its larger energy bandgap at the Γ point.

### 3.2.2 | Density of states (DOS)

The total and partial densities of states (DOS) of $Sc_2CdS_4$ and $Y_2CdS_4$ compounds are illustrated in Figure 3 in order to display the contribution of electronic states of Sc/Y, Cd, and S elements. Orbital contributions (as seen from Figure 3) in these compounds are quite similar. For both these compounds close to the Fermi level in valence band maximum toward higher energy, the *p*-orbital of sulfur S atom shows predominant contribution while the *d*-orbitals of Sc/Y atom shows minor contribution. Moreover, toward lower energy in the valence band region near −7.24 eV, the sharp Cd-*d* and smaller S-*p* orbitals appear. Instead of this, toward higher energy in the conduction band, major contribution of Sc/Y-*d* and S-p,*d* orbitals occurred with lesser contribution of Cd-*d* orbitals in both compounds. The VB remains on the Fermi level and CB moves away from the Fermi level in these compounds, going from Sc to Y. From this investigation, we may conclude that the direct energy bandgaps arise in the compounds $Sc_2CdS_4$ and $Y_2CdS_4$ due to S-*p* and Sc/Y-*d* orbitals hybridization, which is further beneficial to electrical transport. The major contribution of S-*p* states in the entire valence band indicates the dominant ionic bonding character with a small covalent part in these compounds.

## 3.3 | Optical properties

Linear optical responses of the compounds were reported in the energy range of 0 to 15 eV as presented in Figure 4A-F.

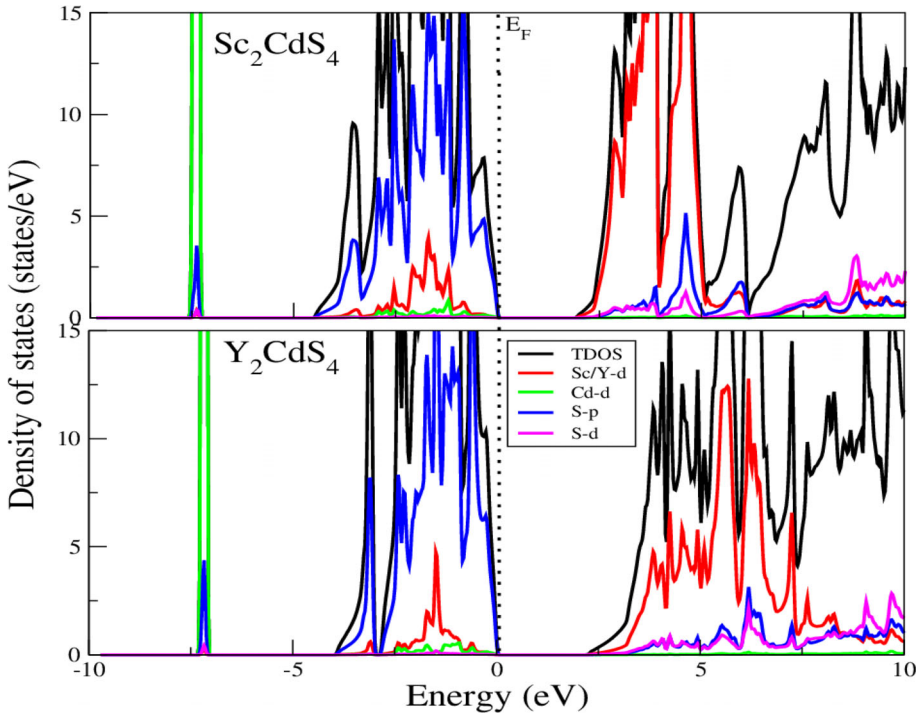


FIGURE 3 Density of states (Total and Partial) of $Sc_2CdS_4$ and $Y_2CdS_4$ compounds calculated with mBJ-GGA [Colour figure can be viewed at wileyonlinelibrary.com]

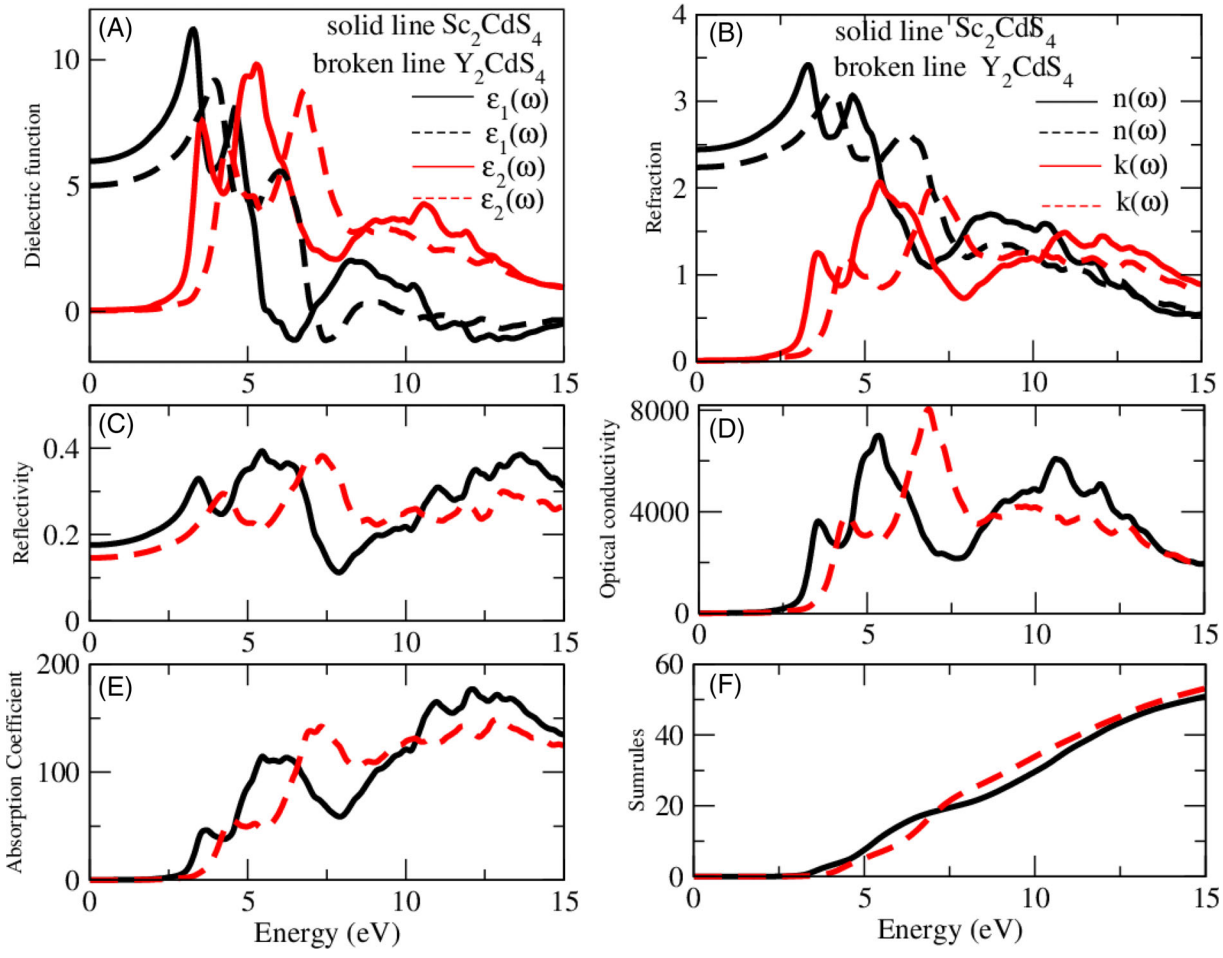


FIGURE 4 (A-F). Optical parameters of $Sc_2CdS_4$ and $Y_2CdS_4$ compounds in the energy range between 0 and 15 eV. The solid lines represent $Sc_2CdS_4$ while the broken lines represent $Y_2CdS_4$ [Colour figure can be viewed at wileyonlinelibrary.com]

The optical response of a material at all photon energies can be expressed by dielectric function $\varepsilon(\omega) = \varepsilon_1(\omega) + i\varepsilon_2(\omega)$.[29] The real part $\varepsilon_1(\omega)$ (denoting the polarizability of the materials) and imaginary part $\varepsilon_2$ (ω) comprised energy loss of light photons by the materials for compounds. The dielectric function for $Sc_2CdS_4$ and $Y_2CdS_4$ compounds is presented in Figure 4A. The spectrum of $\varepsilon_1(\omega)$ for $Sc_2CdS_4$ and $Y_2CdS_4$ compounds starts at low frequency with values of 5.98 and 5.01, which is termed as static dielectric function. It is clearly understandable from the figure that bandgap and the static dielectric constant $\varepsilon_1(0)$ of the compounds are strongly related; that the smaller bandgap produced a larger $\varepsilon_1(0)$ value, when one moves down in the group from Sc to Y followed the Pen model. After the low-frequency region, $\varepsilon_1(\omega)$ increases to a maximum value of 11.13 at 3.32 eV energy for $Sc_2CdS_4$ and 9.14 at 3.97 eV energy for $Y_2CdS_4$, respectively. The main characteristic peaks of the understudy compounds are observed in visible to ultraviolet energy range. Beyond these peaks, $\varepsilon_1$ decreases below zero after the energy of 5.68 eV and 7.10 eV for $Sc_2CdS_4$ and $Y_2CdS_4$ compounds. The compounds exhibited greater energy losses beyond these values after certain energy ranges, where they show metallic behavior of the material. Moreover, it observed that the peaks moved toward higher energies due to the increase in the bandgap when Sc cation is replaced by Y. The calculated results of $\varepsilon_1(\omega)$ are also compared with the recently reported spectra for $Sc_2ZnS_4$ and $Y_2ZnS_4$[30] as shown in Figure S1. The real part of dielectric function for the Cd-based spinel compounds is slightly lower than the Zn-based spinel compounds due to its larger energy bandgap. Overall, the spectra of Cd-based compounds follow the pattern of the Zn-based spinels.

The imaginary part $\varepsilon_2(\omega)$ of $Sc_2CdS_4$ and $Y_2CdS_4$ compounds is shown in Figure 4A. The curves for $\varepsilon_2(\omega)$ show that its starting point is $E_o = 2.10$ eV for $Sc_2CdS_4$ and 2.34 for $Y_2CdS_4$. Prominent peaks appeared beyond the threshold points due to the interband transitions from Cd-*d* and S-*p* states in lower energy region to Sc/Y-*d* states in CB for $Sc_2CdS_4$ and $Y_2CdS_4$, respectively. After the threshold points, the spectra increase monotonically due to larger contribution of joint density of states to $\varepsilon_2(\omega)$. The dominant two peaks appear in both these compound. The maximum absorption capabilities with the main peak of $Sc_2CdS_4$ and $Y_2CdS_4$ have magnitude of 9.704 and 8.734 at energy 5.315 eV and 6.820 eV, respectively. The compounds' absorption main peaks lie in the ultraviolet region while it shifted toward higher energy and become low in moving from Sc to Y. Being a medium bandgap material ($Sc_2CdS_4$ and $Y_2CdS_4$ compounds) showed large absorption covering the entire far visible region together with ultraviolet region. Therefore, the stable and UV-Vis absorbents are promising candidates for optoelectronics technology. The calculated results of $\varepsilon_2(\omega)$ are also compared with the recently reported spectra for $Sc_2ZnS_4$ and $Y_2ZnS_4$[30] as shown in Figure S1. The imaginary parts of $Sc_2CdS_4$ and $Y_2CdS_4$ are found in close agreement with the $Sc_2ZnS_4$ and $Y_2ZnS_4$, respectively. As $Sc_2ZnS_4$ and $Y_2ZnS_4$ have shown high device absorption efficiency,[30] Cd-based spinels can also show high absorption ability.

The calculated refractive index $n(\omega)$ is displayed in Figure 4B. The solid lines represent $Sc_2CdS_4$ while the broken lines represent $Y_2CdS_4$. Interestingly, $n(\omega)$ follows the same behavior as $\varepsilon_1(\omega)$. This similar trend of both spectra is supported by the established theory.[29] The static value $n(0)$ of refractive index was found to be 2.44 for $Sc_2CdS_4$ and 2.24 for $Y_2CdS_4$, following the same behavior as $\varepsilon_1(0)$. The highest peaks of refractive index $n(\omega)_{max}$ appear with having values of 3.407, 3.096 at energy 3.36 eV, 4.04 eV for $Sc_2CdS_4$ and $Y_2CdS_4$ compounds respectively, which are in the ultraviolent region of the electromagnetic spectrum. It is clearly observed that the small bandgap compounds have high refractive index. These results show that $n(0)$ and $n(\omega)_{max}$ decrease by replacing Sc with Y, which means it follows the same trend as $\varepsilon_1(0)$ while opposes the trend present in energy gap of these compounds. Beyond prominent characteristics peaks, refractive index decreases by increasing the photon energy due to small joint density of states participating in the interband transitions.

Extinction coefficients $K(\omega)$ describe the absorption capability of the material when an incident light pass through it. The value of $K(\omega)$ (shown in Figure 4B) starts at the bandgaps of the compounds, then abruptly increases and reaches its maximum peak values with the minor peak appearing on higher energy side of the spectra of both the compounds. The maximum reported values of extinction coefficients $K(\omega)max$ are 2.044 and 1.941 at energy 5.46 eV and 6.87 eV for $Sc_2CdS_4$ and $Y_2CdS_4$ compounds, respectively. The $Sc_2CdS_4$ shows higher value of extinction coefficient, which means it absorbs more light as compared to $Y_2CdS_4$ compound. Moreover, the maximum peaks move toward the higher energies, whereas clear multi-peaks with shoulders appear in both compounds, as well as by replacement of the cations from Sc to Y. This is due to the increase in the energy bandgap of the compounds in going from Sc to Y.

The frequency-dependent reflectivity $R(\omega)$ results are shown in Figure 4C. The static frequency limit of reflectivity $R(0)$ for $Sc_2CdS_4$ is 17% and for $Y_2CdS_4$ is 14%, respectively, which follows the same behavior as $\varepsilon_1(\omega)$, and these compounds exhibited maximum reflectivity values of 39% ($Sc_2CdS_4$) and 38% ($Y_2CdS_4$) in the energy range from 2.5 to 15 eV. Beyond maximum peaks, $\varepsilon_1(\omega)$ goes below zero to reveal the metallic character after the energy 5.68 and 7.10 eV for $Sc_2CdS_4$ and $Y_2CdS_4$

compounds. Based on the reflectivity spectra, these compounds can be used effectively as reflectors in the UV region. Furthermore, it is clear from the spectra of $R(\omega)$ that the static values decrease by changing the cation from Sc to Y. It is due to the fact that the bandgaps of compounds are increased, which also broadens the high reflectivity range of the compounds. From the plot, we can see that $Sc_2CdS_4$ is comparatively a better reflector.

The optical conductivity $\sigma(\omega)$ of $Sc_2CdS_4$ and $Y_2CdS_4$ compounds is shown in Figure 4D. The optical conductivity $\sigma(\omega)$ starts at the bandgap value of the compounds. $\sigma(\omega)$ increases slowly with smaller peaks for both the compounds and then reaches gradually to a maximum value, the maximum values $\sigma(\omega)_{max}$ are 6985.19 $\Omega^{-1}$ $cm^{-1}$ and 7845.69 $\Omega^{-1}$ $cm^{-1}$ for $Sc_2CdS_4$ and $Y_2CdS_4$ compounds at energy 5.38 eV and 6.87 eV, respectively. $Y_2CdS_4$ compound possesses higher $\sigma(\omega)$ than $Sc_2CdS_4$. After reaching maximum values, it starts decreasing with multiple minor peaks in the high energy range. Compounds show prominent optical conductivity in the UV region, and consequently these systems can be functional for the high-frequency devices operating in this range.

The absorption coefficient $\alpha(\omega)$ is important in describing the intensity of the light in the medium and optical density. Figure 4E depicts the absorption coefficient spectra of $Sc_2CdS_4$ and $Y_2CdS_4$ compounds. It starts at the critical point and then increases above these compounds with characteristic optical structures originated due to the electronic transitions with high joint density of states. The maximum values of $\alpha(\omega)$max for $Sc_2CdS_4$ and $Y_2CdS_4$ compounds are $175.71 \times 10^4$ $cm^{-1}$ and $148.52 \times 10^4$ $cm^{-1}$ at energy 12.1 eV and 13 eV, respectively. $Sc_2CdS_4$ compound possesses higher $\alpha(\omega)$ than $Y_2CdS_4$. It shows that the absorption strength is decreased by replacing Sc with Y for the compounds.

The effective numbers of electrons (per unit cell) that take part in both inter and intra-band transitions contributing to the valence band can be studied by sum rules. It is obvious from Figure 4F that electrons start to contribute significantly in interband transitions at around 3.50 eV and 4.07 eV for $Sc_2CdS_4$ and $Y_2CdS_4$. Beyond these values, $N_{eff}$ increases for higher energies, and it becomes higher for $Y_2CdS_4$ beyond 7 eV compared to $Sc_2CdS_4$, which is also seen in the dielectric function spectra. The continuous increase of effective electrons with the increase of energy up to 15 eV indicates that interband transitions contribute significantly to these compounds.

## 3.4 | Thermoelectric properties

In order to have promising thermoelectric properties in a material, it is important to have a large value of Seebeck coefficient (S) and electrical conductivity, while extremely low thermal conductivity. Here, we have important thermoelectric parameters at the temperature interval 300 K $\leq T \leq$ 800 K.

It is noticed from Figure 5 that the Seebeck coefficient shows a decreasing trend with temperature for $Sc_2CdS_4$ and $Y_2CdS_4$ compounds. The Seebeck coefficient for both the compounds starts from the high positive values 249.5 μV/K for $Sc_2CdS_4$ and 237.92 μV/K for $Y_2CdS_4$ compounds at about 300 K. It should be noted that the Seebeck coefficient is affected by temperature, that is, when temperature increases, a significant decrease of (S) is observed with a value of 234.7 μV/K and 219.14 μV/K for $Sc_2CdS_4$ and $Y_2CdS_4$ compounds at around 800 K. $Sc_2CdS_4$ and $Y_2CdS_4$ compounds exhibit p-type conduction behavior due to its positive values over the whole temperature range. Furthermore, $Sc_2CdS_4$ compound possesses a high value of Seebeck coefficient than $Y_2CdS_4$ over the whole temperature range.

We have reported the electrical conductivity of $Sc_2CdS_4$ and $Y_2CdS_4$ compounds, which is shown in Figure 6. The figure depicts that the electrical conductivity values increased monotonously from its minimum value with the increasing temperature. The increasing value of electrical conductivity clearly shows the semiconducting nature of these. The lowest values reported for $Sc_2CdS_4$ and $Y_2CdS_4$ compounds are $1.971 \times 10^{18}$ (1/Ωms) and $2.500 \times 10^{18}$ (1/Ωms) at a temperature of about 300 K, while the highest values reported for $Sc_2CdS_4$ and $Y_2CdS_4$ compounds are $8.575 \times 10^{18}$ (1/Ωms) and $9.448 \times 10^{18}$ (1/Ωms), respectively, at a temperature of about 800 K. Furthermore, $Y_2CdS_4$ compound

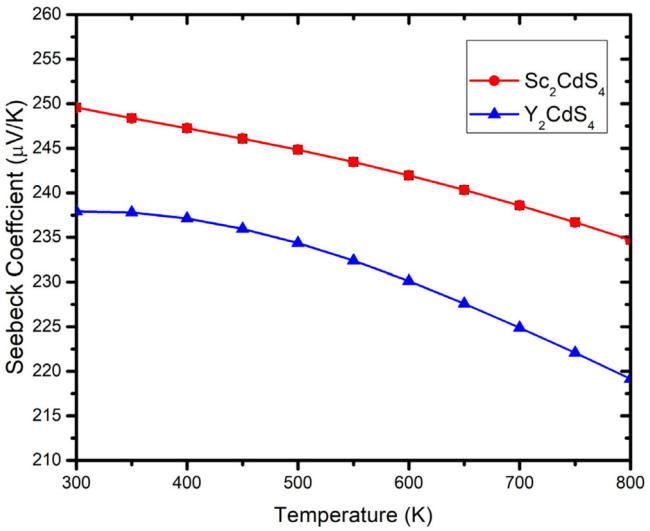


FIGURE 5 Variation in Seebeck coefficient with respect to temperature for $Sc_2CdS_4$ and $Y_2CdS_4$ compounds [Colour figure can be viewed at wileyonlinelibrary.com]

possesses the greatest value of electrical conductivity than $Sc_2CdS_4$ over the whole temperature range.

The electronic thermal conductivity for $Sc_2CdS_4$ and $Y_2CdS_4$ compounds is plotted in Figure 7A. The thermal conductivity monotonically increases with temperature over the entire temperature range. At 300 K, it starts to increase gradually with values of $0.480 \times 10^{14}$ and $0.565 \times 10^{14}$ W/mKs and finally reaches its higher values of $4.857 \times 10^{14}$ and $4.640 \times 10^{14}$ W/mKs at about 800 K for $Sc_2CdS_4$ and $Y_2CdS_4$ compounds. Wiedemann-Franz law is obeyed in these compounds for variations in conductivities. Moreover, $Y_2CdS_4$ compound possesses a high value of thermal conductivity than $Sc_2CdS_4$ till 650 K; furthermore, both the compounds share the value of 3.658 W/mKs of thermal conductivity at a temperature of 700 K while at the end of the temperature of about 800 K $Y_2CdS_4$ lag behind $Sc_2CdS_4$, which is clearly observed in the plots.

Lattice thermal conductivity (LTC) is an important thermoelectric parameter that signifies the contribution of phonon toward heat flow. Due to the limitation of BoltzTraP computational code, we have calculated LTC of $Sc_2CdS_4$ and $Y_2CdS_4$ compounds through Slack equation[31] and depicted in Figure 7B.

$$K_L = A\frac{\Theta_D^3 V_{\text{tot}}^{1/3}\bar{M}}{\gamma^2 n^{2/3} T t} \quad (1)$$

where $\gamma$ is the Grüneisen parameter, $A$ is $\gamma$ reliant coefficient ($\sim 3.1 \times 10^{-6}$ for $K_L$ in W/mKs), $\bar{M}$ *is* the average atomic mass (in amu), $V$ is the volume of the primitive unit cell (in a.u$^3$), $n$ is the total number of atoms per unit cell, $T$ is temperature (in K), $\Theta_D$ is Debye temperature (in K),[32] and $t$ is the relaxation time. The values of $\Theta_D$ (412.7 for $Sc_2CdS_4$ and 355.6 K for $Y_2CdS_4$) and $\gamma$ (2.35 for both the compounds) are calculated through Quasi-harmonic Debye approximation.[33] The values of $\Theta_D$ and $\gamma$ at 0 GPa pressure and 0 K temperature, calculated through this model, are similar to those computed from elastic constants.[34] Figure 8 shows that the LTC for both the compounds decreases with increase in temperature. Similar behavior is also reported in other semiconductor

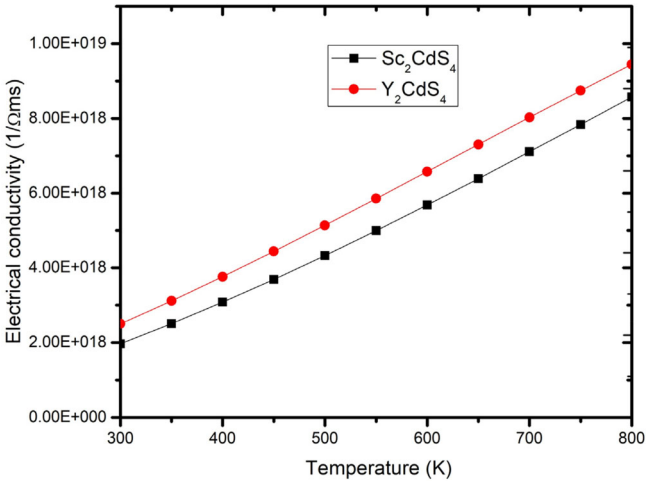


**FIGURE 6** Variation in electrical conductivity with respect to temperature for $Sc_2CdS_4$ and $Y_2CdS_4$ compounds [Colour figure can be viewed at wileyonlinelibrary.com]

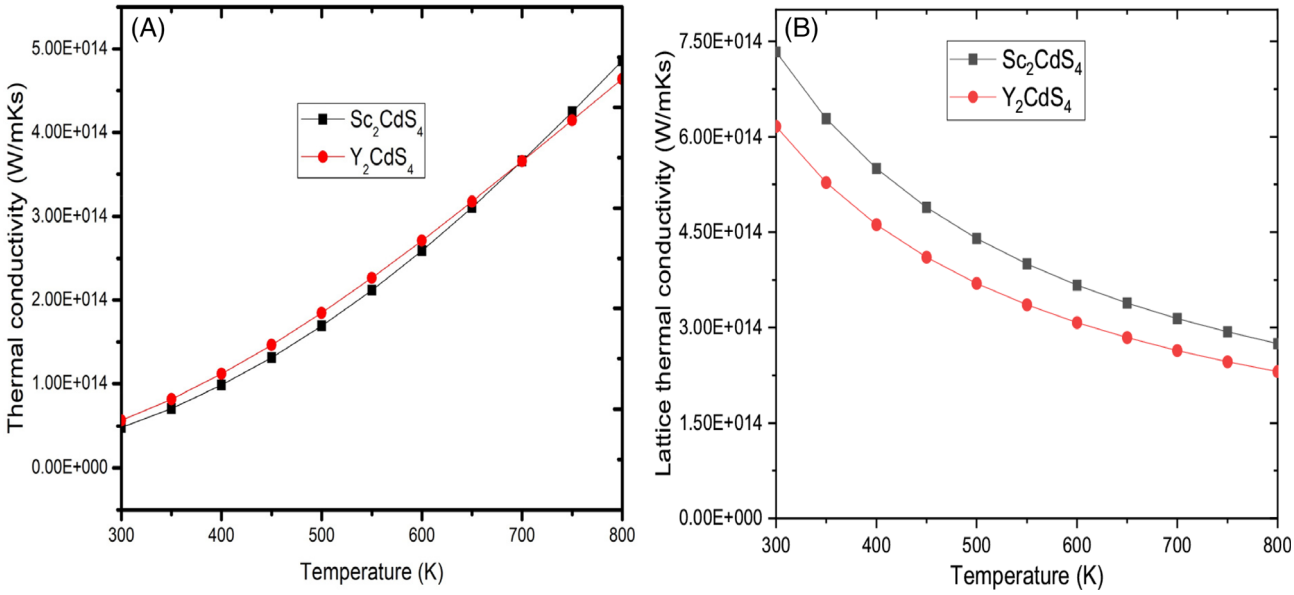


**FIGURE 7** Variation in thermal conductivity of (A) electrons (B) lattice, with respect to temperature for $Sc_2CdS_4$ and $Y_2CdS_4$ compounds [Colour figure can be viewed at wileyonlinelibrary.com]

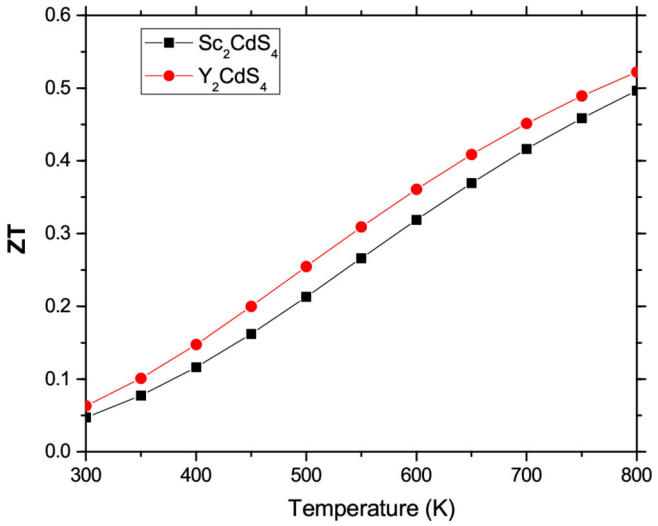


FIGURE 8 Calculated figure of merit (ZT) of the compounds from room temperature to 800 K [Colour figure can be viewed at wileyonlinelibrary.com]

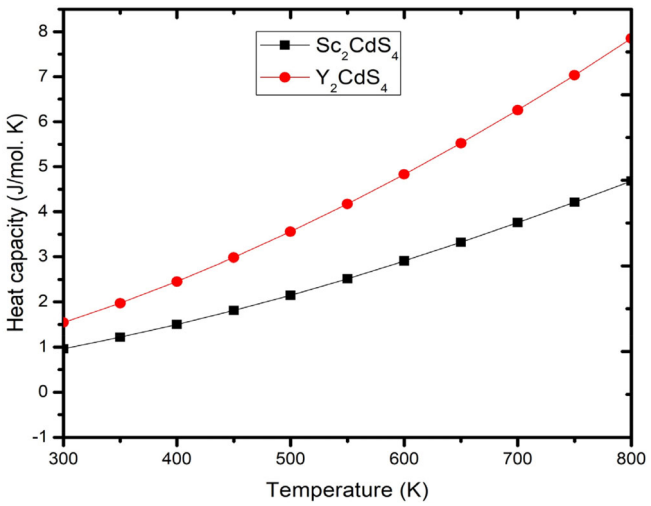


FIGURE 9 Variation in specific heat with respect to temperature for $Sc_2CdS_4$ and $Y_2CdS_4$ compounds [Colour figure can be viewed at wileyonlinelibrary.com]

materials.[35,36] In the present calculation, the LTC values of $Sc_2CdS_4$ and $Y_2CdS_4$ vary from $7.3\times10^{14}$ and $6.1\times10^{14}$ W/mKs at 300 K to $2.2\times10^{14}$ and $1.8\times10^{14}$ W/mKs.

It is important to know the efficiency of the materials for thermal energy conversion. The figure of merit (ZT) characterizes the materials' efficiency to heat conversion. Therefore, it is calculated and presented in Figure 8. It is observed that $Y_2CdS_4$ has higher figure of merit compared to $Sc_2CdS_4$ throughout the temperature range (300-800 K). It is due to its lower LTC compared to $Sc_2CdS_4$. It starts below 0.1 at room temperature and enhances with the increase in temperature and reaches its maximum value (about 0.5) at 800 K.

Figure 9 shows the heat capacity ($C_V$) of the compounds in temperature range of 300 to 800 K. At 300 K, it started to gradually increase with values of 0.959 and 1.545 J/mol K and finally reaches its maximum values of 4.679 and 7.852 J/mol K at about 800 K for $Sc_2CdS_4$ and $Y_2CdS_4$ compounds. Overall, the trend of variation of Cv is similar to thermal and electrical conductivities (Figures 6 and 7A). The escalation of $C_V$ in the studied temperature range shows that it obeys Dulong-Petit and $T^3$ law in the low and high temperature range, respectively. Furthermore, $Y_2CdS_4$ compound possesses the greatest value of heat capacity than $Sc_2CdS_4$ over the whole temperature range.

## 4 | CONCLUSIONS

First-principles calculations of structural, electronic, optical, and thermoelectric properties of ternary *d*-metal sulfides $Sc_2CdS_4$ and $Y_2CdS_4$ compounds were investigated by using FP-LAPW+lo method. Geometrical optimization was carried out using the GGA. Both compounds show semiconducting nature and direct bandgap with a value of 1.886 eV for $Sc_2CdS_4$ and 2.209 eV for $Y_2CdS_4$, respectively. The compounds are found optically active in the visible and UV regions. Comparatively, $Sc_2CdS_4$ shows better optical response in the visible region than $Y_2CdS_4$. The thermoelectric properties were also studied in the temperature range between 300 and 800 K. $Y_2CdS_4$ compound has the highest electrical conductivity at high temperature. Both the compounds $Sc_2CdS_4$ and $Y_2CdS_4$ are *P*-type thermoelectric materials with ZT of about 0.5. Appropriate direct energy gap and figure of merit indicate the possible applications of these compounds for energy conversion devices.

## ACKNOWLEDGEMENTS

Murefah Mana Al-Anazy extends her sincere appreciation to the Deanship of Scientific Research at Princess Nourah bint Abdulrahman University through the Fast-track Research Funding Program. The research (for A. Laref) was supported by a grant from the "Research centre of the Female Scientific and Medical Colleges", Deanship of Scientific Research, King Saud University.

## CONFLICT OF INTEREST

The authors declare no competing financial interests.

## DATA AVAILABILITY STATEMENT

Data sharing is not applicable to this article as no datasets were generated or analyzed during the current study (the article describes entirely theoretical research).

## ORCID

*Ali H. Reshak* https://orcid.org/0000-0001-9426-8363
*Ghulam Murtaza* https://orcid.org/0000-0001-5520-2265
*Amel Laref* https://orcid.org/0000-0003-1689-7724


## REFERENCES


1. Moheimani NR, Parlevliet D. *Renew Sustain Energy Rev*. 2013;27:494-504.
2. Murtaza G, Hussain S, Faizan M, et al. Anion-cation replacement effect in lead free tin based variant perovskites. *Phys B Condensed Matter*. 2020;595:412345.
3. Ali R, Hou GJ, Zhu ZG, Yan QB, Zheng QR, Su G. Stable mixed group II (Ca, Sr) and XIV (Ge, Sn) lead-free perovskite solar cells. *J Mater Chem A*. 2018;6:9220-9227.
4. Güllü HH. Analysis of forward and reverse biased current–voltage characteristics of $Al/Al_2O_3$/n-Si Schottky diode with atomic layer deposited $Al_2O_3$ thin film interlayer. *Bull Mater Sci*. 2019;42:89.
5. Zhang S, Liwei S, Chuanfu H, Wangsuo X, Lanyang Z, Haiyan Z. Effects of biaxial strains and high pressure on the structural, electronic, and vibrational properties of DC-$HgM_2Te_4$ (M = Al, In). *Phys Status Solidi*. 2018;255:1700574.
6. Nii Y, Sagayama H, Arima T, et al. Orbital structures in spinel vanadates $AV_2O_4$ (A= Fe, Mn). *Phys Rev B*. 2012;86:125142.
7. Zhang K, Zhen C, Wei W, et al. Insight into metallic behavior in epitaxial half-metallic $NiCo_2O_4$ films. *RSC Adv*. 2017;7:36026-36033.
8. Telegin AV, Sukhorukov YP, Loshkareva NN, et al. Giant magnetotransmission and magnetoreflection in ferromagnetic materials. *J Magnet Magnet Mater*. 2015;383:104-109.
9. Punam S, Ludi M, Ilan S, Xiaolan Z, Jin H, Dae HK. Metal insulator transition with ferrimagnetic order in epitaxial thin films of spinel $NiCo_2O_4$. *Appl Phys Lett*. 2012;100:032102.
10. Khan AU, Orabi RARA, Pakdel A, et al. Sb Doping of metallic $CuCr_2S_4$ as a route to highly improved thermoelectric properties. *Chem Mater*. 2017;29:2988-2996.
11. Zienert T, Fabrichnaya O. Thermodynamic assessment and experiments in the system MgO–$Al_2O_3$. *CAL*. 2013;40:1-9.
12. Liao F, Han X, Zhang Y, Han X, Xu C, Chen H. Hydrothermal synthesis of mesoporous $MnCo_2O_4/CoCo_2O_4$ ellipsoid-like microstructures for high-performance electrochemical supercapacitors. *Ceram Int*. 2019;45:7244-7252.
13. Laura E, Andreana P, Patrizia M, Stefano M. A thermodynamic approach to obtaining transparent spinel ($MgAl_2O_4$) by hot pressing. *J Eur Ceram Soc*. 2015;35:651-661.
14. Saravanan M, Sabari Girisun TC. Enhanced nonlinear optical absorption and optical limiting properties of superparamagnetic spinel zinc ferrite decorated reduced graphene oxide nanostructures. *Appl Surf Sci*. 2017;392:904-911.
15. Luchechko A, Kravets O. Novel visible phosphors based on $MgGa_2O_4$-$ZnGa_2O_4$ solid solutions with spinel structure co-doped with Mn2+ and Eu3+ ions. *JOL*. 2017;192:11-16.
16. Barathiraja C, Manikandan A, Mohideen AU, Jayasree S, Antony SA. Magnetically recyclable spinel $MnxNi_1-xFe_2O_4$ (x= 0.0–0.5) nano-photocatalysts: structural, morphological and opto-magnetic properties. *J Superconduct Novel Magnetism*. 2016;29:477-486.
17. Tripathi VK, Nagarajan R. Rapid synthesis of mesoporous, nano-sized $MgCr_2O_4$ and its catalytic properties. *J Am Ceram Soc*. 2016;99:814-818.
18. Fu G, Wang J, Chen Y, et al. Exploring indium-based ternary thiospinel as conceivable high-potential air-cathode for rechargeable Zn–Air batteries. *Adv Energy Mater*. 2018;8:1802263.
19. Peskov MV, Blatov VA. Comparative crystal-chemical analysis of binary compounds and d-block metal halides containing tetrahedral anions. *Zh Neorg Khim*. 2004;49(7):1137.
20. Santamaría-Pérez D, Amboage M, Manjón FJ, et al. crystal chemistry of $CdIn_2S_4$, $MgIn_2S_4$, and $MnIn_2S_4$ thiospinels under high pressure. *J Phys Chem C*. 2012;116:14078-14087.
21. Muhammad R, Shuai Y, Tan HP. First-principles study on hydrogen adsorption on nitrogen doped graphene. *Physica E*. 2017;88:115-124.
22. Muhammad R, Shuai Y, Tan HP. A first-principles study on alkaline earth metal atom substituted monolayer boron nitride (BN). *J Mater Chem C*. 2017;5(32):8112-8127.
23. Rafique M, Shuai Y, Tan HP, Muhammad H. Theoretical perspective on structural, electronic and magnetic properties of 3d metal tetraoxide clusters embedded into single and di-vacancy graphene. *Appl Surf Sci*. 2017;408:21-33.
24. Canepa P, Bo SH, Gautam GS, et al. High magnesium mobility in ternary spinel chalcogenides. *Nat Commun*. 2017;8:1-8.
25. Lee TD, Ebong AU. A review of thin film solar cell technologies and challenges. *Renew Sustain Energy Rev*. 2017;70:1286-1297.
26. Blaha P, Schwarz K, Madsen G, Kvasnicka D, Luitz J. *An augmented plane wave plus local orbitals program for calculating crystal properties*. Austria: Vienna University of Technology; 2011.
27. Perdew JP, Burke K, Ernzerhof M. Generalized gradient approximation made simple. *Phys Rev Lett*. 1996;77:3865.
28. Tran F, Blaha P. Accurate band gaps of semiconductors and insulators with a semilocal exchange-correlation potential. *Phys Rev Lett*. 2009;102:226401.
29. Murtaza G, Ahmad I, Amin B, et al. Investigation of structural and optoelectronic properties of $BaThO_3$. *Opt Mater*. 2011;33:553-557.
30. Saeed M, Noor Z, Ali R, et al. Prediction of novel $X_2ZnZ_4$(X = Sc, Y; Z = S, se) spinels materials for renewable energy applications. *Int J Energy Res*. 2021;1-9.
31. Slack GA. The effect of rare-earth filling on the lattice thermal conductivity of skutterudites. *Solid State Phys*. 1979;34:1.
32. Morelli DT, Jovovic V, Heremans JP. Intrinsically minimal thermal conductivity in cubic I– V– VI 2 semiconductors. *Phys Rev Lett*. 2008;101:035901.
33. Blanco MA, Francisco E, Luania V. GIBBS: isothermal-isobaric thermodynamics of solids from energy curves using a quasi-harmonic Debye model. *Comput Phys Commun*. 2004;158:57.
34. Dar SA, Srivastava V, Sakalle UK, Khandy SA. Ab initio investigation on electronic, magnetic, mechanical, and thermodynamic properties of AMO 3 (A= Eu, M= Ga, In) perovskites. *J Supercond Nov Magn*. 2018;31:1549.
35. Ali MA, Alshahrani T, Murtaza G. Defective perovskites $Cs_2SeCl_6$ and $Cs_2TeCl_6$ as novel high temperature potential thermoelectric materials. *Mater Sci Semicond Process*. 2021;127:105728.

36. Ali MA, Reshak AH, Murtaza G, et al. Optoelectronic and transport properties of Rb/$Cs_2TeI_6$ defective perovskites for green energy applications. *Int J Energy Res*. 2020;1-8. https://doi.org/10.1002/er.6378.

## SUPPORTING INFORMATION

Additional supporting information may be found online in the Supporting Information section at the end of this article.

**How to cite this article:** Khan AA, Reshak AH, Noor Z, et al. First-principles calculations of structural, electronic, optical, and thermoelectric properties of ternary *d*-metal sulfides $Sc_2CdS_4$ and $Y_2CdS_4$ compounds. *Int J Energy Res*. 2021;1–11. https://doi.org/10.1002/er.6695